Supporting Information

Modulating the Photodynamic Modality of Au_{22} Nanoclusters Through Surface Conjugation of Arginine for Promoted Healing of Bacteria-Infected Wound

Xinyue Dou[a], Sariah Saalah[a], Chel-Ken Chiam[a], Jianping Xie*[b], and Coswald Stephen Sipaut*[a]*

[a]*Chemical Engineering Programme, Faculty of Engineering, Universiti Malaysia Sabah, Kota Kinabalu 88400, Sabah, Malaysia*

E-mail: jojoba2021@126.com (X.D.); css@ums.edu.my (C.S.S.)

[b]*Department of Chemical and Biomolecular Engineering, National University of Singapore, 4 Engineering Drive 4, Singapore, 117585, Singapore*

E-mail: chexiej@nus.edu.sg (J.X.)

1. Materials and methods

1.1 Chemical reagents, bacteria, and animals

Chloroauric acid ($HAuCl_4 \geq 99.9$ %), sodium hydroxide (NaOH, ≥ 96 %), ethanol (C_2H_5OH, ≥ 99.0 %), hydrochloric acid (HCl), arginine (Arg), cupric sulfate ($CuSO_4$) and glutathione (GSH) were purchased from Sinopharm Chemical Reagent Co., Ltd. Sodium borohydride ($NaBH_4$, ≥ 96 %) were purchased from Shanghai Shanpu Chemical Co., Ltd (China). Formalin solution was purchased from Merck. 1-(3-dimethylaminopropyl)-3-ethylcarbodiimide hydrochloride (EDC; ≥98%), vancomycin

(Van), N-hydroxysuccinimide (NHS; ≥98%), 3-(4,5-dimethylthiazol-2-yl)-2,5-diphenyltetrazolium bromide (MTT), Fe^{2+}-$(MGD)_2$ (MGD: N-methyl-D-glucamine dithiocarbamate), dichlorodihydrofluorescein diacetate (DCFH-DA) dye, 2,9-dimethyl-1,10-phenanthroline (DMP), 5,5-dimethyl-1-pyrroline N-oxide (DMPO) and dimethyl sulfoxide (DMSO) were purchased from Sigma-Aldrich. Ultrapure water was used throughout the experiments.

Phosphate buffer solution (PBS) solution, Luria-Bertani (LB) nutrient agar, and LB broth were purchased from Qingdao Hope Bio-Technology Co., Ltd. A complete Dulbecco's modified Eagle medium (DMEM) was purchased from Beijing Solarbio Science & Technology Co., Ltd. Standard strains of *Staphyloccocus aureus* ATCC 6538 (*S. aureus*) and *Escherichia coli* ATCC 25922 (*E. coli*) were purchased from China General Microbiological Culture Collection Center.

The animals were purchased from China Weitong Lihua Animal Co., LTD., and female ICR mice aged 6 weeks were selected. Animals were maintained under specific pathogen-free conditions and fed ad libitum. Animal experiments were conducted according to the international ethics guidelines and the National Institutes of Health Guide concerning the Care and Use of Laboratory Animals.

1.2 Instrumentation

The size and morphology of samples were observed by transmission electron microscope (TEM, JEM-2100 Plus Electron Microscope). The optical properties of Au_{22} NCs and Arg-Au_{22} NCs and the turbidity of bacteria were measured by UV-vis absorption spectroscopy on a Shimadzu UV-1800 spectrometer. The

photoluminescence (PL) spectra of samples were acquired on a PerkinElmer LS-55 fluorescence spectrometer. The molecular formula of Au_{22} NCs was analyzed on a Bruker Impact II (electrospray ionization mass spectrometry) ESI-MS system operating in negative ion mode. Zeta (ζ) potential tests were conducted on a Zetasizer Nano ZS (Malvern Co., England) system. The valance band (VB)-X-ray photoelectron spectra (VB-XPS) were obtained on an ESCALAB MK II Axis Ultra Dld system using Al Kα as an exciting source. The PL decay profiles were gained on a transient photoluminescence spectrometer (FLS-1000, Edinburgh Instruments Ltd.). Hematoxylin/eosin (H&E) stained images were taken on an inverted fluorescence microscope (OLYMPUS IX73). Electronic paramagnetic resonance (EPR) spectra were recorded on an electron paramagnetic resonance spectrometer (EPR200-Plus, Guoyi Quantum (Hefei) Technology Co., LTD).

1.3 Reactive oxygen species (ROS) assay

The H_2O_2 concentration was determined using the DMP method, whereby a centrifuge tube containing 0.3 mL of DMP (ethanol, 10 mg/mL) and 0.3 mL of $CuSO_4$ (water, 0.01 mol/L) was used. Following this, 0.3 mL of the reaction solution was added to the tube. The mixture was then incubated for 10 min at room temperature with O_2 bubbled, after which the H_2O_2 concentration was determined by measuring the absorbance of the supernatant liquid solutions at 454 nm.

1.4 Reactive nitrogen species (RNS) assay

The RNS were measured by Electron Paramagnetic Resonance (EPR, EPR200-Plus). The trapping agent of RNS, Fe^{2+}-$(MGD)_2$, was used it right after it was ready. Fresh

solution of Fe^{2+}-$(MGD)_2$ was prepared by dissolving MGD and ferrous sulfate heptahydrate in deoxy deionized water and the final concentration was fixed to be 5 mM. Before EPR test, 0.1 mL Fe^{2+}-$(MGD)_2$ was added into 0.5 mL sample solution at dark or illumination for 10 min. EPR spectral simulation was conducted by the system equipped from the instrument.

1.5 Cytotoxicity assessment

The *in vitro* cytotoxicity of pristine Au_{22} NCs and Arg-Au_{22} NCs was evaluated by a MTT assay. The L929 cells were selected as cell models. Firstly, the cells were seeded into a 96-well plate with a concentration of 1×10^4 cells/well and cultured for 48 h. Subsequently, different concentrations of Au_{22} NCs or Arg-Au_{22} NCs were added to each well and incubated for 24 h at 37 °C. Afterwards, 20 μL of MTT solution was added to each well and continued to incubate for 4 h at 37 °C. Finally, the absorbance of each well was measured at 460 nm by Tecan Spark® multimode microplate readers.

1.6 Animal experiments

This study was performed in strict accordance with the NIH guidelines for the care and use of laboratory animals (NIH Publication No. 85–23 Rev. 1985) and was approved by the Biomedical Ethics Committee of Qingdao Zhong Hao Biological Engineering Co., Ltd. (Qingdao, China). The mice were randomly assigned to 6 groups according to the samples with 5 mice in each group: control (PBS), Light, Van, Au_{22}-Light, Arg-Au_{22} NCs and Arg-Au_{22}-Light. The mice were anesthetized with isoflurane (2%) and removed back hair with a depilatory cream. A skin biopsy perforator (8 mm

in diameter) was used to create a full-thickness wound on the pasteurized dorsal skin. The wound sites were inoculated with *E. Coli* suspensions (100 μL, 10^8 CFU/mL), covered by 3M films, and left for 1 day to develop the severe infection. Subsequently, the infected wounds were treated with various photodynamic antibacterial agents (200 μL, 1 mg mL^{-1}). Afterwards, the infected wounds were irradiated by a commercial 300 W Xenon lamp with an optical cut-off filter (λ = 400-1100 nm, 100 mW/cm^2, CEL-HXF300, Beijing China Education AuLight Technology (CEAuLight) Co., Ltd.) for 5 min each day. After being treated for eleven days, all mice were sacrificed and the surrounding wound tissues were collected and fixed in paraformaldehyde (4%) for further H&E staining. Blood was collected and used to detect the levels of IL-6, IL-1β, and TNF-α.

1.7 Levels of inflammatory cytokines in blood homogenates for efficacy evaluation

The security indexes of Arg-Au_{22} NCs were tested using ELISA kits (Corning). Blood samples were obtained from the mice on the last day of experiment.

1.8 Histological analysis

The collected skin tissue and organ samples were fixed for 48 h, then dehydrated and paraffin embedded. Paraffin sections with thickness of 5 μm were prepared for histological analysis. Hematoxylin eosin (H&E) staining was used for observation.

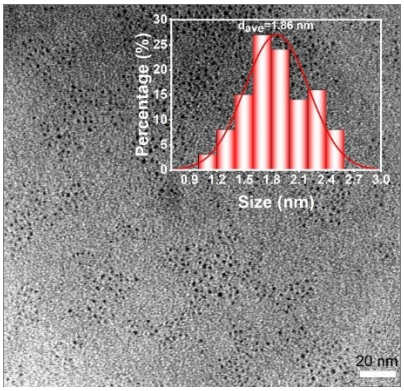

Figure S1. A representative TEM image and size distribution histogram (inset) of pristine Au_{22} NCs.

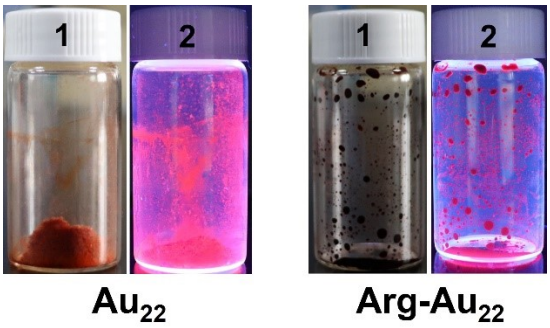

Figure S2. Digital photos of pristine Au_{22} NCs and Arg-Au_{22} NCs in solid state under visible (item #1) and UV (item #2) light illumination.

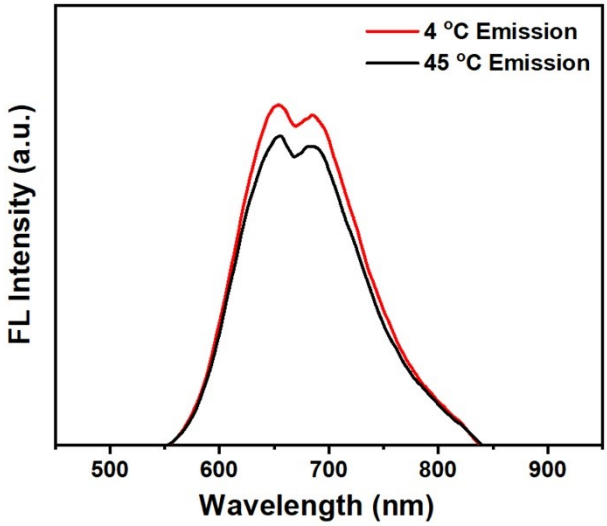

Figure S3. Photoemission spectra of the Arg-Au_{22} NCs at 4 °C (red curve), and 45 °C (black curve).

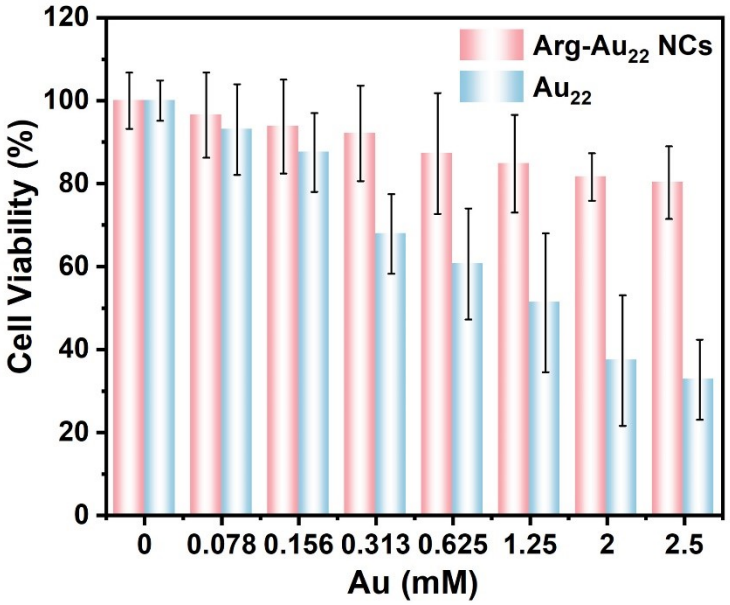

Figure S4. L929 Cell viability evaluated by MTT assay after 24 h treatment with different concentrations of Arg-Au_{22} NCs and Au_{22} NCs.

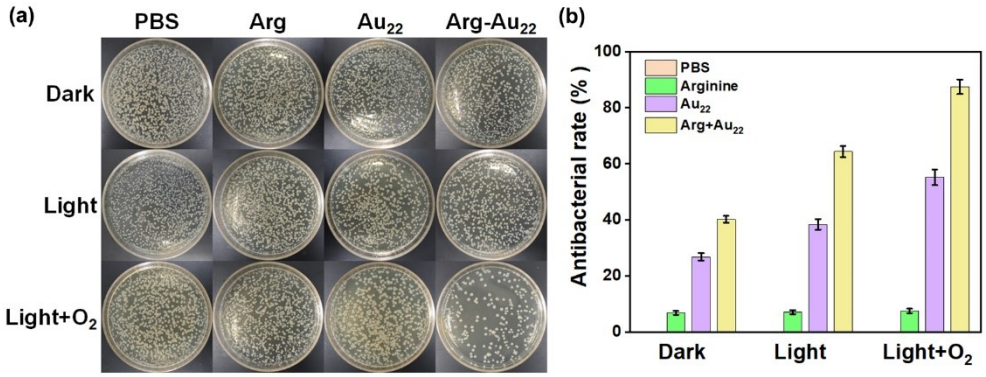

Figure S5. (a) Fungus colony growth of Monilia albicans treated with PBS, Arg, Au_{22} NCs and Arg-Au_{22} NCs under the conditions of dark, visible-light illumination in the air, visible-light illumination with O_2 bubbling. (b) Antifungal activities of different samples against Monilia albicans.

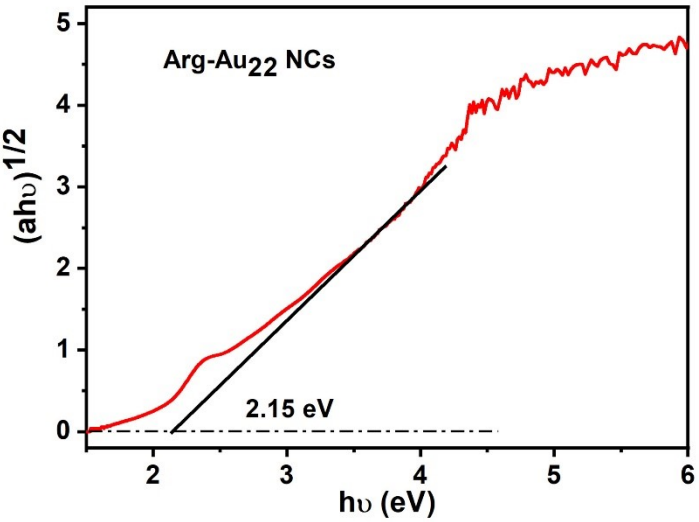

Figure S6. The Tauc plot of Arg-Au_{22} NCs acquired based on their UV-vis absorption spectrum.

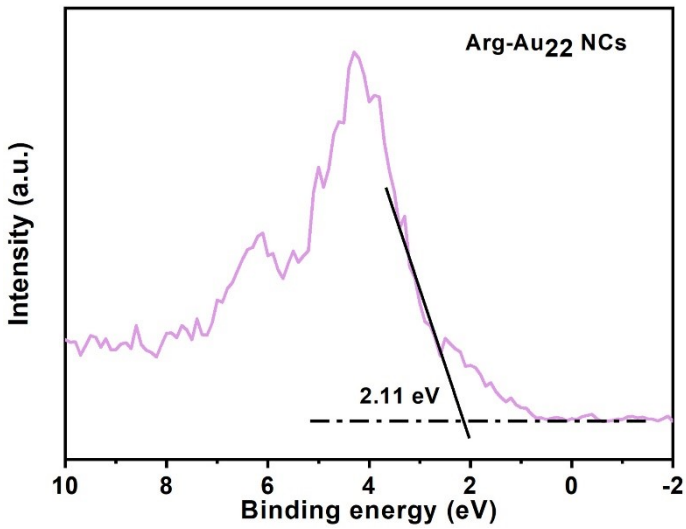

Figure S7. XPS of valence band (VB-XPS) of Arg-Au_{22} NCs.

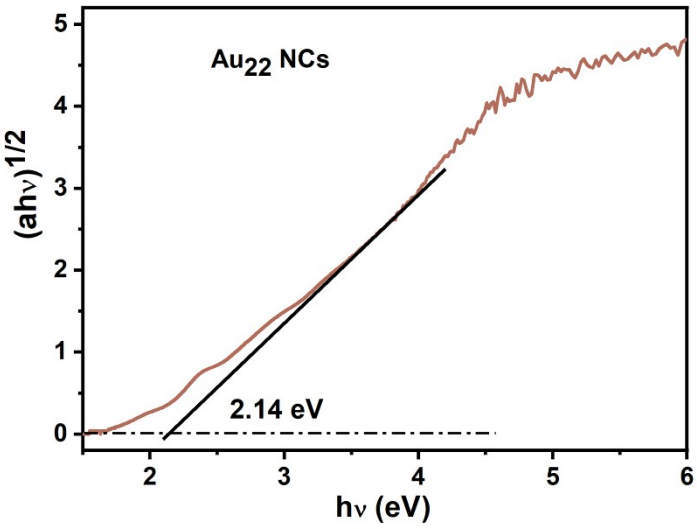

Figure S8. The Tauc plot of pristine Au_{22} NCs acquired based on their UV-vis absorption spectrum.

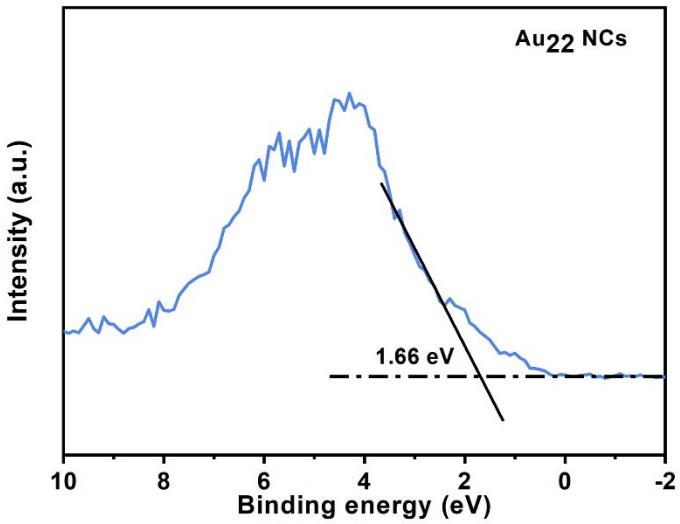

Figure S9. XPS of valence band (VB-XPS) of pristine Au_{22} NCs.

Supplementary Note I:

The VB-XPS (Figure S7 and S9) shows that the valence band (VB) of the Au_{22} NCs and Arg-Au_{22} NCs are respectively at 1.66 eV and 2.11 eV, which could be converted to 1.77 V and 2.22 V vs RHE based on the formula $E_{RHE} = \varphi + E_{VB\text{-}XPS}$ - 4.44 eV (RHE: reversible hydrogen electron, φ: work function, 4.55 eV). In addition, the Tauc plots

(Figure S6 and S8) of Au_{22} NCs and Arg-Au_{22} NCs were transformed from the Figure 1b, and the band gaps were gained about 2.14 eV for Au_{22} NCs and 2.15 eV for Arg-Au_{22} NCs. Therefore, the position of the CB of the Au_{22} NCs and Arg-Au_{22} NCs are determined to be - 0.37 V vs RHE and 0.07 V vs RHE, respectively. While the VB-CB band of pristine Au_{22} NCs encompasses the potentials required for oxygen or H_2O_2 reduction ($O_2/•O_2^-$, −0.33 V vs. RHE, pH=7; O_2/H_2O_2, 0.28 V vs. RHE, pH=7; $H_2O_2/•OH$, 0.73 V vs. RHE, pH=7), that of Arg-Au_{22} NCs make them incapable of producing $•O_2^-$ because of the lower potential for $•O_2^-$ generation. The corresponding reaction formula potentials, and conditions are displayed below.

$O_2+e^- \rightarrow O_2•^-$, - 0.33 V vs. NHE, pH = 7.

$O_2 + 2e^- + 2H^+ \rightarrow H_2O_2$, + 0.28 V vs. NHE, pH = 7.

$H_2O_2 + e^- + H^+ \rightarrow •OH + H_2O$, + 0.73V vs. NHE, pH = 7.

$H_2O \rightarrow •OH + 2H^+ + 2e^-$, + 1.97 V vs. NHE, pH = 7.

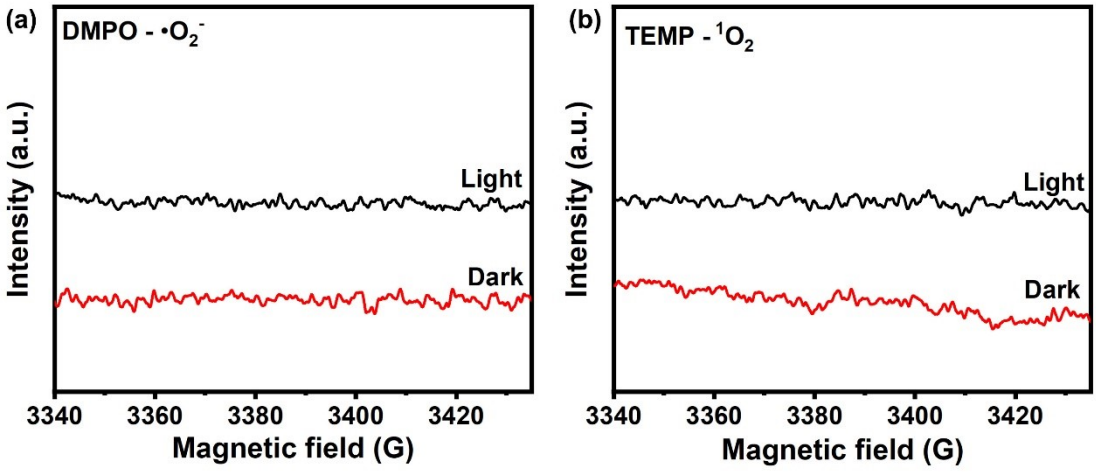

Figure S10. Electronic paramagnetic resonance (EPR) spectra of (a) $•O_2^-$ and (b) $^1O_2$ of Arg-Au_{22} NCs with or without visible light illumination.

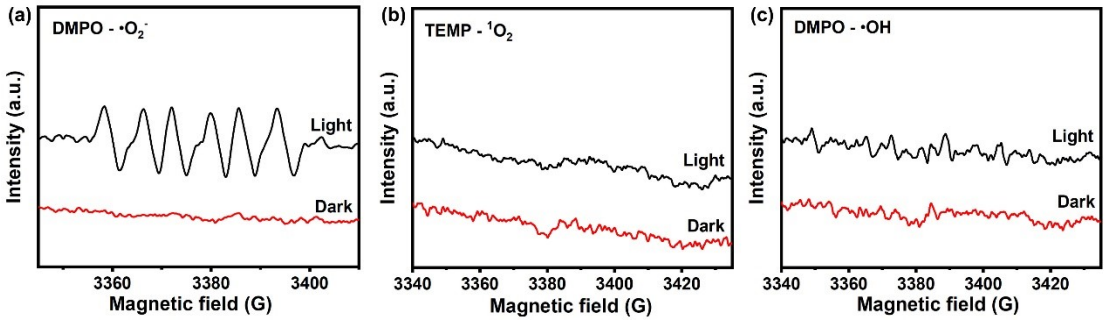

Figure S11. Electronic paramagnetic resonance (EPR) spectra of (a) $\bullet O_2^-$, (b) $^1O_2$ and (c) of •OH of pristine Au_{22} NCs with or without visible light illumination.

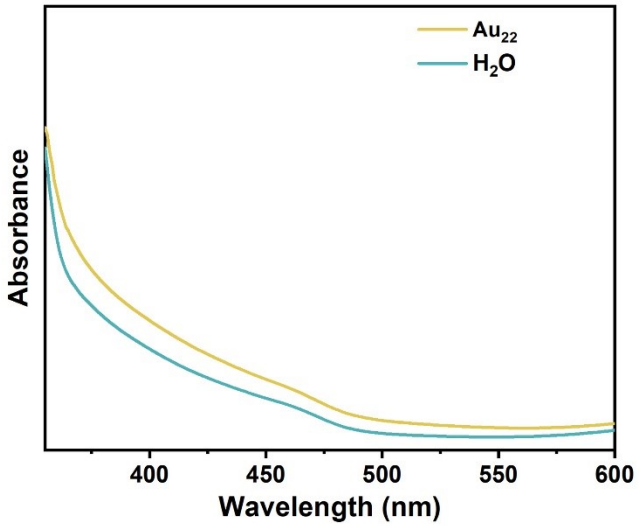

Figure S12. Photodynamic production of H_2O_2 by pristine Au_{22} NCs under visible light illumination for 60 min.

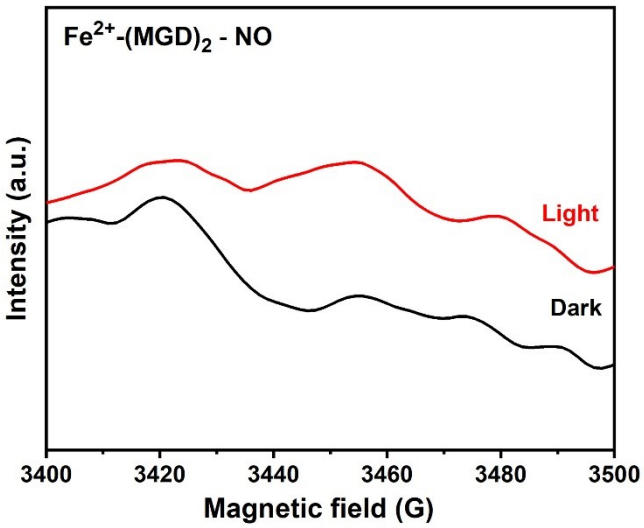

Figure S13. EPR spectra of NO of pristine Au_{22} NCs with or without visible light illumination.

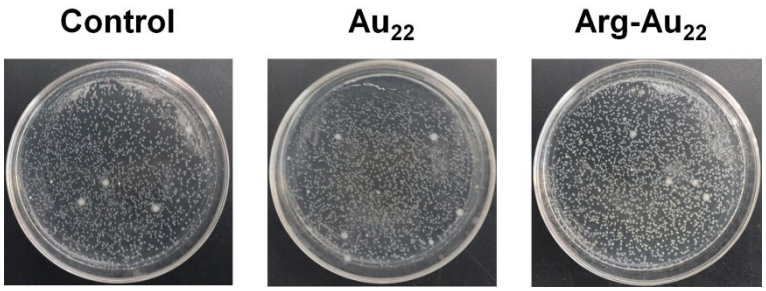

Figure S14. (a) Bacterial colony growth of *E. coli* treated with PBS (control), Au_{22} NCs in the presence of ROS scavenger (DMPO), and Arg-Au_{22} NCs in the presence of ROS scavenger (DMPO) under the condition of visible-light illumination and O_2 atmosphere for 1 h.

Supplementary Note II:

In order to distinguish the specific antibacterial contributions of ROS, RNS, and intrinsic antibacterial Au species, a series of antibacterial tests were conducted on Arg-Au_{22} NCs, pristine Au_{22} NCs, and PBS as a control, under varying experimental

conditions. These conditions included darkness, visible light exposure in the presence of O_2 bubbling, with and without ROS scavenger DMPO (as illustrated in Figure S14 and Figure 2). Using Arg-Au_{22} NCs as a case study, the antibacterial efficacy of Arg-Au_{22} NCs in darkness and under O_2 bubbling was considered as the inherent antibacterial activity of the Arg-Au_{22} species. Moreover, the antibacterial activity of Arg-Au_{22} NCs subjected to light exposure and O_2 bubbling in the presence of DMPO was interpreted as the combined antibacterial effects of RNS and the inherent antibacterial activity of the Arg-Au_{22} species. By comparing the antibacterial outcomes of Arg-Au_{22} NCs under light exposure and O_2 bubbling with or without DMPO, the antibacterial contributions of ROS could be obtained. Of note, the antibacterial contribution of RNS calculated in this manner, is severely underestimated because the RNS is originated from the Arg oxidation by ROS and thus the DMPO-mediated ROS exhaustion made the Arg-oxidation-directed RNS production insufficient. Nevertheless, the Figure of the specific antibacterial contributions of ROS, RNS, and intrinsic antibacterial Au species could provide a general insight on the photodynamic antibacterial mechanism. Similarly, the specific antibacterial effects of ROS and intrinsic antibacterial Au species of pristine Au_{22} NCs were quantified using analogous methodologies.